Technical Report
RAL-TR-2001-018

CLRC

The Orbital Magnetization of a Mott Insulator, V_2O_3, Revealed by Resonant X-Ray Bragg Diffraction

S W Lovesey K S Knight and D S Sivia

15th March 2001

COUNCIL FOR THE CENTRAL LABORATORY OF THE RESEARCH COUNCILS

Enquiries about copyright, reproduction and requests for additional copies of this report should be addressed to:

The Central Laboratory of the Research Councils
Library and Information Services
Rutherford Appleton Laboratory
Chilton
Didcot
Oxfordshire
OX11 0QX
Tel: 01235 445384 Fax: 01235 446403
E-mail library@rl.ac.uk

ISSN 1358-6254

The orbital magnetization of a Mott insulator, V_2O_3, revealed by resonant x-ray Bragg diffraction

S. W. Lovesey, K. S. Knight and D. S. Sivia

ISIS Facility, Rutherford Appleton Laboratory,
Oxfordshire OX11 0QX, UK

Abstract

Structure factors calculated for x-ray Bragg diffraction by magnetically ordered vanadium sesquioxide, V_2O_3, with signal enhancement from the vanadium K-shell resonance, are compared with data gathered in azimuthal-angle scans at space-group forbidden reflections. Diffraction enhanced by a K-shell resonance reveals properties of the orbital magnetization in the valence shell of the resonant ion whereas other core states, which have two partners because of the spin-orbit interaction, reveal properties of both the spin and orbital magnetization in the valence shell. Agreement on all issues between observed and calculated Bragg intensities support the use of an atomic model for the interpretation of data. The reflections are shown to be purely magnetic, and associated with the orbital magnetic moment and the octupole moment of a vanadium ion. Reflections with the Miller index h even are analysed to give the canting angle of the magnetic easy-axis. Data from the rotated ($\pi'\sigma$) and unrotated ($\sigma'\sigma$) channels of scattering provide an angle consistent with an earlier interpretation of magnetic neutron diffraction. With h odd diffraction enhanced by an E1 event is forbidden. Intensities enhanced by an E2 event are from anistropic components of the octupole moment, and the dominant contribution has three-fold rotational symmetry which is an imprint of the high-temperature trigonal structure. Analysis of azimuthal-angle scans, with h even and h odd, provides estimates of orbital moments that in the future can be confronted with *ab initio* calculations of the electronic properties of V_2O_3. By and large, the complicated pattern of azimuthal-angle scans can be attributed to the low symmetry (monoclinic) structure adopted below the Néel temperatures.

PACS numbers: 71.30. + h, 75.50.Ee, 78.70. Ck

Keywords: vanadium sesquioxide, orbital magnetism, resonant x-ray Bragg diffraction.

1. Introduction

Vanadium sesquioxide (V_2O_3) displays a number of electronic, magnetic and structural properties that are challenging to interpret and explain [1 – 7]. At room temperature V_2O_3 has the corundum structure with space group $R\bar{3}c$, and it is metallic and paramagnetic. (It is unique among the iso-structural sesquioxides with respect to its small *a/c* ratio and metallic conductivity.) On reducing the temperature the corundum structure distorts to a monoclinic structure with space group *I*2/*a*. The structural transition in the temperature range 150 – 160K is strongly first-order and destructive. Accompanying the transition are a change from metallic to insulating behaviour and the onset of antiferromagnetic order [3]. The metal-insulator transition is viewed as a classic Mott transition, in which spin and orbital degrees of freedom are independent.

Recently, results from resonant x-ray Bragg diffraction experiments [8 – 10] have added to the wealth of knowledge about V_2O_3. We put forward an explanation of some key aspects of the observed x-ray diffraction pattern [11] in which intensity is enhanced by the resonance at the K-edge of a vanadium ion. Here, we give a more complete account of the model employed and the work involved in calculating structure factors for resonance enhanced Bragg diffraction. New calculations, for azimuthal-angle scans, are also reported and they are shown to provide a fully quantitative explanation of available data [8 –10]. The success of our model in explaining the resonant x-ray diffraction data permits us to draw specific conclusions about the orbital magnetization present in V_2O_3.

The data of interest has been gathered for Bragg reflections that are forbidden by the space group, and often called charge-forbidden reflections. In general, such reflections are due to spatial anisotropy in the charge distribution or a long-range magnetic order that is not indexed on the chemical structure. When long-range magnetic order is absent, the diffraction at charge-forbidden reflections is usually referred to as Templeton-Templeton scattering [12, 13]. Intensities measured for different settings of the crystal rotated about the Bragg wavevector can provide direct information on the nature of the anisotropy and spatial symmetry. Tuning the primary x-ray energy to an inner- shell absorption edge makes the diffraction signal specific to the resonant ion, and for the case in hand this is a vanadium ion. Should the Bragg wavevector coincide with an axis of rotation through the site occupied by the resonant ion the azimuthal-angle (ψ) meshes with the rotational periodicity, and the Bragg intensity displays a periodicity in ψ equal to twice the degree of the axis of rotation [14, 15].

Such a configuration can be achieved in diffraction from the corundum structure [11,14] and the observed azimuthal-angle scan is six-fold periodic. Broadly speaking, complexity in azimuthal-angle scans observed for magnetically ordered V_2O_3 [8 – 10] is due to the low spatial symmetry of the monoclinic structure adopted by the crystal. While the symmetry of the site occupied by a resonant vanadium ion carries a heavy imprint of a three-fold axis of rotation, that controls properties in the corundum structure [11], monoclinic Bragg wavevectors do not coincide with the trigonal axis of the corundum structure and it is this mismatch, between the wavevectors and the axis of rotation, that is largely responsible for the seemingly complex pattern of the azimuthal-angle scans. However, we can demonstrate that the scans do contain some very specific information on the orbital magnetization of V_2O_3.

The resonance enhanced intensity is related to properties of the valence shell that accommodates the photo-ejected core electron in the intermediate state of the elastic scattering process. Absorption at the K-edge and an electric-dipole event (E1) gives access to valence states with atomic p-like character, and an electric quadrupole event (E2) at the same edge gives access to d-like states ($1s \rightarrow 3d$). We analyse in terms of a pure E2 event diffraction data collected with the primary energy tuned to a feature in the pre-edge (5.464 keV and $\lambda = 2.27$Å) of the vanadium K-shell. The associated Bragg intensity is therefore attributed directly to properties of the 3d-shell of a vanadium ion. As a function of the primary energy, the observed intensity is adequately described by a single oscillator. In this instance, we can confidently ascribe the intensity to orbital degrees of freedom [16] and spin degrees of freedom are not explicitly contributing. For magnetically ordered V_2O_3 we have demonstrated that charge-forbidden reflections are due to the orbital magnetization [11] (specifically, the amplitude is the mean value of spherical tensors of odd rank that are odd with respect to time reversal). The intensity must decrease on warming the sample and vanish with the loss of magnetic long-range order. For the corundum structure adopted in the high-temperature (paramagnetic) phase of V_2O_3 charge forbidden reflections are due to an orbital tensor of rank four, i.e. the orbital hexadecapole [11].

There are two main ingredients in the calculated structure factors. First, knowledge of the chemical and magnetic structures. Information on the crystal structure, which is based on observations reported by Dernier and Marezio [2], is gathered in section 2 together with the configuration of magnetic moments [3]. The second ingredient is a model of resonance-enhanced Bragg diffraction. We employ an atomic model which should be adequate for a one-component intensity profile like the ones observed with V_2O_3 at the vanadium K-shell pre-edge

[8, 9]. After adopting a single oscillator to describe the intensity profile the amplitude attached to the oscillator can be calculated without further approximation [16]. The atomic model for the event 1s → 3d, which is of interest to us here, shows that the amplitude is constructed from spherical tensors that describe the orbital properties of the 3d-shell. After putting together the two ingredients it only remains to describe the geometry of the experiment, namely, the orientation of the crystal (a function of the azimuthal angle) in the frame of reference used for the polarizations and wavevectors of the primary and diffracted beams of x-rays. These aspects of the calculation of the structure factors for unrotated ($\sigma'\sigma$) and rotated ($\pi'\sigma$) channels of scattering are described in sections 3 and 4. Thereafter, in section 5, we confront the structure factors with experimental data and, in section 6, draw conclusions about resonant x-ray Bragg diffraction by vanadium sesquioxide.

2. Chemical and magnetic structures

At room temperature vanadium sesquioxide has a trigonal (corundum) structure with space group 167 ($R\bar{3}c$). Lowering the temperature of the material induces distortions which include tilting of the trigonal (hexagonal-c) axis and reduction of the point-group symmetry of sites occupied by vanadium ions from $3(C_3)$ to that of no symmetry.

The space group of the low temperature monoclinic structure is number $15(I2/a)$ in which vanadium ions occupy sites 8 (f). This is a body-centred cell and Bragg wavevectors $\boldsymbol{\tau}_m(hkl)$ for charge reflections have the necessary condition $h + k + l$ an even integer. (Miller indices h, k and l are integers.) In neutron diffraction patterns, magnetic reflections are indexed by $h + k + l$ odd [3] and Table I contains the corresponding spatial phase factors for the Bragg structure factor. The antiferromagnetic configuration of vanadium magnetic moments, displayed in Fig. 1, consists of sheets of moments with ferromagnetic alignment within $(010)_m$ layers, or hexagonal (110) layers, and moment reversal between adjacent layers. The moments are orientated along some easy-axis in these layers, and we take ϕ as the canting angle with respect to the trigonal axis.

The trigonal basis vectors are $\mathbf{a}_h = a(1, 0, 0)$, $\mathbf{b}_h = a(-\frac{1}{2}, \frac{1}{2}\sqrt{3}, 0)$ and $\mathbf{c}_h = c(0, 0, 1)$ and the volume of the unit cell = $a^2c\sqrt{3}/2$. Following Dernier and Marezio [2]in the use of an I - centred cell, from these vectors we generate monoclinic basis vectors $\mathbf{a}_m = (0, \frac{1}{\sqrt{3}}\ 2\ a, \frac{1}{3}\ c)$,

$\mathbf{b}_m = \mathbf{a}_h$ and $\mathbf{c}_m = (0, \frac{1}{\sqrt{3}}\ a, -\frac{1}{3}\ c)$, and the volume of the cell = $a^2c/\sqrt{3}$. The corresponding Bragg wavevector $\tau_m(hkl) \equiv (hkl)_m$ is,

$$\tau_m(hkl) = \tfrac{1}{a}(k, \tfrac{1}{\sqrt{3}}(h+l), \tfrac{a}{c}(h-2l)). \qquad (2.1)$$

We note that $(l0\bar{l})_m$ is parallel to $\mathbf{c}_h$ and $(2lkl)_m$ is normal to $\mathbf{c}_h$.

Referring to Fig. 1, the position coordinates of vanadium ions labelled (1) and (5) are (x, y, z) and $(-x, -y, -z)$, respectively, with $x = 0.3439$, $y = 0.0012$ and $z = 0.2993$ [2]. The positions of the pair (2) and (6) are related by a body-centre translation to the pair (1) and (5). The position coordinates of (3) and (7) are $(\frac{1}{2} - x, y, -z)$ and $(\frac{1}{2} + x, -y, z)$, respectively, and the pairs (4) and (8), and (3) and (7) are related by the body-centre translation. The body-centre translation $(\frac{1}{2},\frac{1}{2},\frac{1}{2})_m = \frac{a}{2}(1, \sqrt{3}, 0)$ and $(\frac{1}{2},\frac{1}{2},\frac{1}{2})_m \cdot \tau_m(hkl) = \frac{1}{2}(h + k + l)$. Spatial phase factors listed in Table I are correct for $h + k + l$ an odd integer, and this condition on Miller indices provides a minus sign in factors for even relative to odd numbered sites. In writing out spatial phase factors in the structure factor it is convenient to define two angles $\nu = 2\pi\ (x, y, z)_m \cdot \tau_m(hkl) = 2\pi\ (xh + yk + zl)$ and $\varepsilon = 4\pi yk$.

3. The structure factor for Bragg diffraction by magnetically ordered V_2O_3

As a function of the energy of the primary x-rays, the observed intensity of diffraction from V_2O_3 which is enhanced by electric-quadrupole (E2) resonance has a simple shape [8, 9] which is adequately described by a single oscillator. In this instance, the integrated intensity can be calculated without approximation [16], and for a pure E2 absorption event 1s $\rightarrow$ 3d the intensity is found to be proportional to the orbital moments of the 3d valence shell. The orbital moments are represented by atomic tensors $\langle \mathbf{T}^{(K)} \rangle$ of rank $K = 0$, 1, 2, 3 and 4. (For electric-dipole absorption the maximum K is 2.) In the structure factor, which is a scalar quantity, the atomic tensors appear in a scalar product with a tensor, denoted by $\mathbf{H}^{(K)}$, that describes the conditions of the primary and diffracted beams of x-rays. It is convenient in the ensuing calculation to consider the quantity,

$$\Psi_Q^{(K)} = \sum_{\mathbf{d}} < T_Q^{(K)}(\mathbf{d}) > \exp(i\boldsymbol{\tau} \cdot \mathbf{d}), \qquad (3.1)$$

where $-K \le Q \le K$, $\mathbf{d}$ defines the position of a resonant vanadium ion in the unit cell and τ is the Bragg wavevector for the reflection in question. With this notation the structure factor is [16, 17]

$$F(\boldsymbol{\tau}) = \sum_{K} (2K+1)^{1/2} \mathbf{H}^{(K)}.\boldsymbol{\Psi}^{(K)} = \sum_{K,Q} (2K+1)^{1/2} (-1)^{Q} H^{(K)}_{-Q} \Psi^{(K)}_{Q} . \qquad (3.2)$$

The components $H^{(K)}_{Q}$ for unrotated ($\sigma'\sigma$) and rotated ($\pi'\sigma$) radiation are tabulated [17]. The tensor $\mathbf{H}^{(K)}$ and $\Psi^{(K)}$ are evaluated in the coordinate system that defines the experimental geometry. Referring to Fig. 2, σ-polarization is perpendicular to the plane of scattering and parallel to the z-axis, and $\hat{\mathbf{q}} - \hat{\mathbf{q}}' = -2\sin\theta\,\hat{\mathbf{x}}$ and $\hat{\mathbf{q}} + \hat{\mathbf{q}}' = 2\cos\theta\,\hat{\mathbf{y}}$ where θ is the Bragg angle.

We find it convenient to consider $\Psi^{(K)}_{Q}$ with respect to orthogonal axes (x,y,z) that include $\mathbf{a}_h = (a,0,0) = \mathbf{b}_m$ and $\mathbf{c}_h = (0,0,c)$. Thereafter we apply to $\Psi^{(K)}_{Q}$ rotations that describe the orientation of the crystal in the coordinates of the experimental geometry that apply to $\mathbf{H}^{(K)}$.

The spatial phase factors in $\Psi^{(K)}_{Q}$ are listed in Table I, and the eight resonant vanadium ions are labelled according to the scheme shown in Fig 1. Following the discussion in section 2, the chemical environments of ions in the pairs (1) & (2), (5) & (6), (7) & (8) and (3) & (4) are taken to be identical. Moreover, the axes of quantization of ions in a pair are oppositely aligned and, in consequence, their atomic tensors differ by a phase factor $(-1)^K$. These two features of the four pairs of ions are incorporated in the atomic tensors listed in Table I. Using the information in this table one finds for (3.1) the result,

$$\begin{aligned} \Psi^{(K)}_{Q} = \{1-(-1)^{K}\}\{ & e^{iv}[< T^{(K)}_{Q}(1) > +(-1)^{h} e^{-i\varepsilon} < T^{(K)}_{Q}(7) >] \\ & + e^{-iv}[< T^{(K)}_{Q}(5) > +(-1)^{h} e^{i\varepsilon} < T^{(K)}_{Q}(3) >]\}. \end{aligned} \qquad (3.3)$$

Evidently, the structure factor for charge-forbidden reflections ($h + k + l$ odd) is constructed from atomic tensors with $K = 1$ and $K = 3$. The odd-rank tensors are purely magnetic and $\langle \mathbf{T}^{(1)} \rangle = \langle \mathbf{L} \rangle / \sqrt{30}$ and $\langle \mathbf{T}^{(3)} \rangle = \langle \Lambda \rangle / 3\sqrt{70}$ where $\langle \mathbf{L} \rangle$ and $\langle \Lambda \rangle$ are, respectively, the orbital magnetic moment and the orbital octupole moment of the 3d-valence shell of a resonant vanadium ion.

Vanadium ions at sites (1) & (5) are related by inversion. The atomic tensor, and **L**, is unchanged by inversion and thus $< T_Q^{(K)}(1) > = < T_Q^{(K)}(5) >$. A similar relation holds for (3) & (7). Using this information in (3.3), and taking K to be an odd integer, one finds,

$$\Psi_Q^{(K)} = 4\{\cos(\nu) < T_Q^{(K)}(1) > + (-1)^h \cos(\nu - \varepsilon) < T_Q^{(K)}(7) >\}. \qquad (3.4)$$

Ions at sites (1) & (7) are related by an a-glide that includes reflection in the $\mathbf{a}_m$ - $\mathbf{c}_m$ plane, which is normal to $\mathbf{a}_h = \mathbf{b}_m$. Reflection in the $\mathbf{a}_m$ - $\mathbf{c}_m$ plane amounts to the change $x \rightarrow -x$, and with it $< T_Q^{(K)} > \rightarrow (-1)^K < T_{-Q}^{(K)} >$. For $K = 1$ $(L_x, L_y, L_z) \rightarrow (L_x, -L_y, -L_z)$, so that reflection in the $\mathbf{a}_m$ - $\mathbf{c}_m$ plane is accompanied by a change in the orientation of the orbital magnetization. The configuration of moments determined by Moon [3] is preserved if the polarity of the local field is now reversed, leading to $(L_x, -L_y, -L_z) \rightarrow (-L_x, L_y, L_z)$, for according to Moon $\langle L_x \rangle = 0$ and the moments are confined to the $\mathbf{a}_m$ - $\mathbf{c}_m$ plane. Reversing the polarity of the local field, which is sometimes described as time-reversal, introduces in the atomic tensor a phase factor $(-1)^K$. The appropriate relation between tensors at sites (1) and (7) is seen to be the union of reflection in the $\mathbf{a}_m$ - $\mathbf{c}_m$ plane and time-reversal, and our discussion leads to the result $\langle T_Q^{(K)}(7) \rangle = \langle T_{-Q}^{(K)}(1) \rangle$; for simplicity of notation, we hereafter write $< T_Q^{(K)} > = < T_Q^{(K)}(1) >$.

In $\Psi_Q^{(K)}$ the phase angle ε is very small and strong reflections are adequately described with $\varepsilon = 0$. On using in (3.4) our result for the atomic tensor for the vanadium ion at site (7) we arrive at,

$$\Psi_Q^{(K)} = 4\cos(\nu)\{< T_Q^{(K)} > + (-1)^h < T_{-Q}^{(K)} >\}. \qquad (3.5)$$

The result (3.5) applies for $h + k + l$ odd (a charge-forbidden reflection) and K odd (purely magnetic diffraction), and it is the basis of the subsequent interpretation of azimuthal-angle scans performed on magnetically ordered V_2O_3. According to (3.5), reflections with h even are described by $\Psi_Q^{(K)} = \Psi_{-Q}^{(K)}$, whereas for h odd $\Psi_Q^{(K)}$ is an odd function of Q and $\Psi_0^{(K)} = 0$.

In the monoclinic structure, sites occupied by the vanadium ions possess no spatial symmetry and one can choose any set of axes for the associated atomic tensors. When

proceeding from the corundum structure to the monoclinic one the average vanadium-oxygen distance remains essentially constant. This aspect of the structural transition, and others mentioned in section 2, indicate that in the monoclinic structure the potential field experienced by a vanadium ion is principally referred to the trigonal axis, $\mathbf{c}_h$, and the field is almost subject to the requirement of a three-fold axis of rotation. An atomic tensor invariant with respect to a three-fold rotation is zero unless the projection index Q has the values 0 or $\pm$ 3. Additions to the potential field, which reduce the symmetry from C_3 to one of no spatial symmetry, lift the restriction on the allowed values of Q.

At the first level of approximation, we can assume that the atomic tensor is diagonal with respect to principal axes in the monoclinic unit cell, and this means $< T_q^{(K)} >_m = \delta_{q,0} < T_0^{(K)} >_m$. The atomic tensor $< T_Q^{(K)} >$ which arises in the structure factor calculated with (3.5) is defined with respect to orthogonal axes that contain $\mathbf{a}_h = \mathbf{b}_m$ and $\mathbf{c}_h$. Following findings from Moon [3], the magnetic easy-axis is taken to lie in the plane normal to $\mathbf{a}_h$ and cant at an angle ϕ with respect to $\mathbf{c}_h$. The relation between $< T_Q^{(K)} >$ and $< T_q^{(K)} >_m$ is then,

$$< T_Q^{(K)} >= \sum_q D_{qQ}^{(K)}(\tfrac{\pi}{2},\phi,-\tfrac{\pi}{2}) < T_q^{(K)} >_m = D_{0Q}^{(K)}(\tfrac{\pi}{2},\phi,-\tfrac{\pi}{2}) < T_0^{(K)} >_m, \qquad (3.6)$$

where $D_{qQ}^{(K)}(\alpha,\beta,\gamma)$ is an element of the rotation matrix [18], and the last equality follows if the atomic tensor $< T_q^{(K)} >_m$ is diagonal.

Taking h even in (3.5) use of (3.6) leads to the result,

$$\Psi_Q^{(K)}(h \text{ even}) = 8\cos(\nu) D_{0Q}^{(K)}(\tfrac{\pi}{2},\phi,-\tfrac{\pi}{2}) < T_0^{(K)} >_m . \qquad (3.7)$$

Calculations of the intensity expected on the basis of (3.7) as the crystal is rotated about $\tau_m(hkl)$ are taken up in the next section.

With h odd $\Psi_0^{(K)} = 0$ and we are led to consider $\Psi_{\pm 1}^{(1)}$, and $\Psi_Q^{(3)}$ evaluated for $Q = \pm 1, \pm 2$, and ± 3. Concerning $\Psi_{\pm 1}^{(1)}$ we know that $<L_x> = <L_{-1} - L_{+1}>/\sqrt{2} = 0$, because the magnetic moment is confined to the $\mathbf{a}_m - \mathbf{c}_m$ plane, and from this condition it follows that

$\Psi_{\pm 1}^{(1)} = 0$. For diffraction enhanced by an E1 absorption event, which entails atomic tensors of rank up to $K = 2$, we reach the conclusion that when both $h + k + l$ and h are odd the E1 structure factor is zero. This finding is consistent with the experimental observations [8, 9]. Turning to the case of diffraction enhanced by an E2 event we are left to consider,

$$\Psi_Q^{(3)}(h \text{ odd}) = 4\cos(\nu)\{< T_Q^{(3)} > - < T_{-Q}^{(3)} >\} = \frac{4}{3\sqrt{70}}\cos(\nu)\sum_q D_{qQ}^{(3)}(\tfrac{\pi}{2},\phi,-\tfrac{\pi}{2}) \tag{3.8}$$

$$\{< \Lambda_q >_m - < \Lambda_{-q} >_m\}.$$

Evidently, here we are considering additions in terms of the octupole moment to the atomic model already employed, in the discussion of diffraction with h even.

4. Azimuthal-angle scans

An azimuthal-angle scan is rotation of the crystal by an angle ψ about the Bragg wavevector τ_m (hkl). Looking along the **x**-axis in Fig. 2 the rotation is in a clockwise direction. The origin $\psi = 0$ is specified by a plane in reciprocal space normal to the plane of scattering. The plane in question is defined by $\boldsymbol{\tau}_m$ and a second Bragg wavevector, which is either $(20\bar{2})_m$ or $(211)_m$. In orthogonal axes that include $\mathbf{a}_h$ and $\mathbf{c}_h$, $(20\bar{2})_m$ is parallel to $\mathbf{c}_h$ and $(211)_m$ is normal to $\mathbf{c}_h$.

4.1 h even

Experimental data is available for azimuthal-angle scans at $(2\bar{2}1)_m$ which is normal to $\mathbf{c}_h$. Writing $\boldsymbol{\tau}_m/|\boldsymbol{\tau}_m| = (t_1, t_2, t_3)$ for $(2\bar{2}1)_m$ one finds $t_1 = -2/\sqrt{7}$, $t_2 = (3/7)^{1/2}$ and $t_3 = 0$. (In the general case, t_1 and t_2 depend on (a/c) and $t_2/t_1 = (h + l)/k\sqrt{3}$.) With $\psi = 0$ the plane defined by $\boldsymbol{\tau}_m$ and $(20\bar{2})_m$ is normal to the plane of scattering. Evidently, with $\psi = 0$ the wavevector $(2\bar{2}1)_m$ can be aligned by rotation about $\mathbf{c}_h$ with the **x**-axis in the experimental geometry, in which $\mathbf{H}^{(K)}$ is defined. The angle of rotation γ about $\mathbf{c}_h$ satisfies $\cos\gamma = -t_1$ and $\sin\gamma = t_2$, and the result (3.7) transforms to,

$$\Psi_{Q'}^{(K)}(h \text{ even}) = 8\cos(\nu) D_{0Q'}^{(K)}(\tfrac{\pi}{2}, \phi, -\tfrac{\pi}{2} - \gamma) < T_0^{(K)} >_m . \qquad (4.1)$$

Rotation of the crystal by ψ about the x-axis is described by the operation of $D_{Q'Q}^{(K)}(\frac{\pi}{2}, \psi, -\frac{\pi}{2})$ on $\Psi_{Q'}^{(K)}$ and the diffracted amplitude in an azimuthal-angle scan is proportional to,

$$\sum_{Q'} D_{Q'Q}^{(K)}(\tfrac{\pi}{2}, \psi, -\tfrac{\pi}{2})\, \Psi_{Q'}^{(K)}\ (h \text{ even}) = 8\cos(\nu)\, D_{0Q}^{(K)}\ (0, \beta_o, \gamma_o - \tfrac{\pi}{2}) < T_0^{(K)} >_m . \qquad (4.2)$$

In reaching this result we have used the addition theorem for components of the rotation matrix [18]. The angles β_o and γ_o are determined by,

$$\cos\beta_o = \cos\phi\cos\psi - \sin\phi\sin\psi\cos\gamma ,$$

and,

$$\cot\gamma_o = -\cos\psi\cot\gamma - \cot\phi\sin\psi/\sin\gamma. \qquad (4.3)$$

As we shall see, these equations determine structure factors to within an overall phase factor that does not influence intensities.

The structure factor $F(\tau_m)$ is calculated from (3.2) and (4.2) and one finds,

$$F(\tau_m) = 8\cos(\nu) \sum_{K=1,3} (2K+1)^{1/2} < T_0^{(K)} >_m \sum_{Q} (-1)^Q H_{-Q}^{(K)}\ D_{0Q}^{(K)}\ (0, \beta_o, \gamma_o - \tfrac{\pi}{2}). \quad (4.4)$$

In the experiments of interest the primary polarization is almost pure σ. Diffraction data have been collected in the unrotated ($\sigma'\sigma$) and rotated ($\pi'\sigma$) channels.

Using results for $H_Q^{(K)}$ listed in [17] the appropriate structure factors of immediate interest are,

$$F_{\sigma'\sigma}(\tau_m) = i\tfrac{2}{5}\cos(\nu)\sin 2\theta\cos\beta_o < L_0 >_m \{1 + \tfrac{1}{3}\frac{< \Lambda_0 >_m}{< L_0 >_m}(3 - 5\cos^2\beta_0)\}, \qquad (4.5)$$

and,

$$F_{\pi'\sigma}(\tau_m) = i\frac{2}{5}\cos(\nu)\sin\beta_o < L_0 >_m \{\cos(3\theta - \gamma_o) + \frac{1}{12}\frac{< \Lambda_0 >_m}{< L_0 >_m}$$

$$[3\cos(3\theta - \gamma_o)(5\cos^2\beta_o - 1) - 5\cos(\theta - 3\gamma_o)\sin^2\beta_o]\}. \quad (4.6)$$

As functions of ψ, fits of $|F(\tau_m)|^2$ to experimental data can provide values for the canting angle and the ratio of the diagonal components of the orbital octupole and magnetic moments. Notice that $F_{\sigma'\sigma}(\tau_m)$ has a simple dependence on the Bragg angle, namely, sin2θ, and with respect to ψ its magnitude is two-fold periodic. In contrast, $F_{\pi'\sigma}(\tau_m)$ is not simple with respect to θ and ψ.

The diffraction pattern observed when neutrons are scattered by magnetically ordered V_2O_3 is indexed with the reflections under discussion in this subsection, and it seems appropriate to consider the physical quantities that can be determined with this technique. In the limit of small Bragg angles, the amplitude for neutron diffraction is proportional to the magnetic moment and its principal component is $\mu_0 = < L_0 + 2S_0 >_m$. Intensities are proportional to $\mu_0^2(1 - k_\zeta^2)$ where k_ζ is the component of $\tau_m / |\tau_m|$ in the direction of the magnetic easy-axis. Moon [3] observed thirteen independent magnetic peaks of which $(010)_m$ is by far the strongest. This finding led Moon to propose that moments lie in the $\mathbf{a}_m - \mathbf{c}_m$ plane, which is normal to $(010)_m$, and one finds $k_\zeta = t_2 \sin\phi + t_3\cos\phi$. By fitting intensities he found $\mu_0 = 1.2 \pm 0.1$ and $\phi = 71°$.

In general, the amplitude for neutron diffraction depends on τ_m, and all the orbital moments of the 3d valence shell up to rank four [19]. For example, the leading contribution made by the octupole moment is proportional to $(5k_\zeta^2 - 1) < \Lambda_0 >_m$, which might be distinguished from the other orbital moments by exploiting the dependence on the direction of τ_m.

4.2 *h* odd

Although the algebra in calculating $F(\tau_m)$ for h odd turns out to be more complicated than for h even the steps involved are the same in both cases. First, $-\tau_m$ is aligned with the x-axis. Values of the Euler angles α, β and γ involved depend on the setting that defines the origin $\psi = 0$. Secondly, the crystal is rotated by ψ about the **x**-axis. For each of the two rotations there is an element of the rotation matrix and in $F(\tau_m)$ the addition theorem reduces these to one component with Euler angles α_o, β_o and γ_o.

The physical quantities that can be extracted, from fits of $|F(\tau_m)|^2$ to experimental data for intensities as a function of ψ, are components of the orbital octupole moment $\langle\Lambda_Q\rangle = \langle\Lambda_Q\rangle' + i\langle\Lambda_Q\rangle''$. More precisely, estimates of the following two ratios can be extracted;

$$r = (\tfrac{3}{5})^{1/2} < \Lambda_{+1} >' / < \Lambda_{+3} >' , \tag{4.7}$$

and

$$t = \sqrt{6} < \Lambda_{+2} >'' / < \Lambda_{+3} >' . \tag{4.8}$$

In arriving at these results we have used the identity $< T_{-Q}^{(K)} >= (-1)^Q < T_Q^{(K)} >^*$.

The two structure factors of interest for analysing data with h odd are;

$$\begin{aligned} F_{\sigma'\sigma}(\tau_m) = \frac{4i}{3\sqrt{5}} < \Lambda_{+3} >' \cos(\nu)\sin 2\theta \sin\beta_o \{\sin^2\beta_o \cos 3(\gamma-\alpha_o) \\ + \tfrac{1}{2} t \sin 2\beta_o \sin 2(\gamma-\alpha_o) + r(5\cos^2\beta_o - 1)\cos(\gamma-\alpha_o)\}. \end{aligned} \tag{4.9}$$

and,

$$F_{\pi'\sigma}(\boldsymbol{\tau}_m) = -\frac{\mathrm{i}}{3\sqrt{5}} < \Lambda_{+3} >' \cos(\nu)\{\sin 3(\gamma-\alpha_o)\,[4\cos A\sin B + \cos B\sin A(1+3\cos 2\beta_o)]$$

$$+\cos 3(\gamma-\alpha_o)\cos\beta_o[4\cos A\cos B\cos^2\beta_o + \sin A\sin B(\cos 2\beta_o - 5)]$$

$$+2t(\sin 2(\gamma-\alpha_o)\sin\beta_o[\sin A\sin B\sin^2\beta_o - 2\cos A\cos B\cos^2\beta_o]$$

$$+\cos 2(\gamma-\alpha_o)\sin 2\beta_o\cos B\sin A) \qquad (4.10)$$

$$+r(\sin(\gamma-\alpha_o)[4\cos A\sin B + \cos B\sin A(1-5\cos 2\beta_o)] + \cos(\gamma-\alpha_o)\cos\beta_o$$

$$[4\cos A\cos B(4-5\cos^2\beta_o) + \sin A\sin B(1-5\cos 2\beta_o)])\}.$$

Here, $A = 2\gamma_o - 2\theta$ and $B = \gamma_o + \theta$. The intensity $|F_{\sigma'\sigma}|^2$ as a function of ψ is two-fold periodic and, in general, $|F_{\pi'\sigma}|^2$ shows no such symmetry.

When the plane defined by $\boldsymbol{\tau}_m$ and $(20\bar{2})_m$ is normal to the plane of scattering the Euler angles satisfy, $t_1 = -\cos\beta\cos\gamma$, $t_2 = \cos\beta\sin\gamma$, $t_3 = -\sin\beta$ and $\alpha = 0$. Note that γ is independent of the cell dimensions. Upon rotation by ψ about the Bragg wavevector $\boldsymbol{\tau}_m$ one needs to determine α_o, β_o and γ_o from,

$$\tan\alpha_o = -\frac{1}{\sin\beta}\tan\psi, \qquad \cos\beta_o = \cos\beta\cos\psi, \qquad \tan\gamma_o = -\tan\beta / \sin\psi. \qquad (4.11)$$

Phases are fixed by conditions derived from the conservation with respect to ψ of the projection of a vector on the **x**-axis, namely,

$$\sin\beta_o\sin\gamma_o = -\sin\beta, \qquad \text{and } \sin\alpha_o\sin\beta_o = \sin\psi. \qquad (4.12)$$

When the plane for the origin $\psi = 0$ is defined by $\boldsymbol{\tau}_m$ and $(211)_m$ one finds $\alpha \neq 0$. In consequence, determination of α, β and γ entails considerable amounts of algebra and we refrain from giving details.

5. A confrontation of experimental data with calculated intensities

Intensities $|F(\tau_m)|^2$ calculated as a function of the azimuthal angle from structure factors for h even, equations (4.5) and (4.6),and h odd, equations (4.9) and (4.10), have been compared with data gathered at the Bragg wavevectors $\tau_m = (2\bar{2}1)_m$, $(111)_m$ and $(30\bar{2})_m$, for which the corresponding Bragg angles calculated with $\lambda = 2.27$Å are $\theta = 36.9°$, 20.8° and 34.2°. Best fits to the data collected at $(2\bar{2}1)_m$ and $(111)_m$ are displayed in Figs. 3 and 4. In this section we describe the fitting scheme and report values deduced for atomic quantities related to the orbital magnetism of V_2O_3.

A confrontation between predictions of the theory and the data requires the input of several parameters. Some can be derived from geometrical considerations, such as Euler and Bragg angles, and are believed to be estimated fairly well; others are experimental in nature, particularly the zero-setting for the azimuthal angle, but are thought to be calibrated reasonably well; some stem from material properties, e.g. r and t, and little is known about their values a priori. These varying degrees of uncertainty are easily taken into account within the Bayesian framework of data analysis [20] and, with suitable commonly-used simplifying assumptions, lead to a somewhat generalized form of least-squares: in addition to a quadratic cost function for a mismatch with the measurements, there is also a penalty for deviating from those parameter-values within the theory which are thought to be known fairly well. The best fits to data shown in Figs. 3 and 4, and at $(30\bar{2})_m$, utilize a robust simplex algorithm [21] for carrying out the (local) optimization.

Referring to Fig. 3, the quality of the fit is better for $(\pi'\sigma)$ than $(\sigma'\sigma)$ and this leads us to give greater credibility to the canting angle, ϕ, deduced from $(\pi'\sigma)$ data. The intensity calculated for $(\sigma'\sigma)$ is two-fold periodic in ψ; the mismatch in the predicted and observed peak positions is not regarded as significant in the interpretation but attributed to ψ-dependent absorption [10]. Although the value of ϕ has not been constrained to be the same in Figs. 3a and 3b, both sets of data are consistent with the angle which has been deduced by magnetic neutron diffraction [3]. While the $(\sigma'\sigma)$ data are not sensitive to $\langle \Lambda_0 \rangle_m / 3\langle L_0 \rangle_m$, the $(\pi'\sigma)$ data indicate that this ratio is small and negative; using $\langle L_0 \rangle_m \sim -0.5$ [8] one finds $\langle \Lambda_0 \rangle_m \sim 0.09$.

Turning to h odd, we have analysed data for $(111)_m$, which is displayed in Fig. 4, and data for $(30\bar{2})_m$ [8, 10]. The quality of the fits is better at $(30\bar{2})_m$ than at $(111)_m$. A signature of this feature of the data sets is that improved fits at $(111)_m$ are obtained on allowing some small lattitude in the Euler angles away from calculated values, namely $\alpha = 0$, $\beta = 12.7°$ and $\gamma = 130.9°$, while the quality of fits at $(30\bar{2})_m$ are barely improved on giving some lattitude to the Euler angles, which are calculated to be $\alpha = -7.0°$, $\beta = -78.4°$ and $\gamma = 121.4°$.

From data in the unrotated channel at $(30\bar{2})_m$ we find $r = 0.81 \pm 0.11$ and $t = 0.03 \pm 0.52$, and from corresponding data in the rotated channel $r = 1.24 \pm 0.24$ and $t = -0.19 \pm 0.13$. Evidently, data in the $(\sigma'\sigma)$ channel are not sensitive to t. Including the results for t obtained from data at $(111)_m$, it appears that $\langle\Lambda_{+2}\rangle''/\langle\Lambda_{+3}\rangle'$ is negative and of magnitude less than one. Bringing together all the values for r we find $\langle\Lambda_{+1}\rangle'/\langle\Lambda_{+3}\rangle' \sim 0.9$.

6. Conclusions

We have calculated structure factors for x-ray Bragg diffraction from magnetically ordered V_2O_3, with signal enhancement from the vanadium K-shell resonance, and successfully compared calculated intensities with data gathered in azimuthal-angle scans at space-group forbidden reflections $(2\bar{2}1)_m$, $(111)_m$ and $(30\bar{2})_m$. As a function of the primary energy of the x-rays the signal observed at 5.464 keV is fully consistent with a single-oscillator model. From this premiss, the x-ray experiments in question reveal exclusively the orbital magnetization of V_2O_3, and quantities not directly obtainable with other experimental techniques.

Calculated structure factors conform to established chemical and magnetic structural properties. At space-group forbidden reflections, the structure factors contain the following additional features.

(a) Reflections are purely magnetic, being associated with atomic moments of the vanadium 3d-valence shell that are odd with respect to the reversal of time. In general, such moments vanish with the loss of long-range magnetic order. Our prediction for V_2O_3 is borne out in experiments which show that intensities decrease with increasing temperature, and vanish at the Néel temperature.

(b) A selection rule on the order of the electric absorption event and Miller indices *h k l*. With $h + k + l$ odd (a space-group forbidden reflection) reflections with h odd do not contain a contribution from an E1 (electric dipole) event, and the finding is in accord with observations. In the reported calculation, the selection rule stems from the actual configuration of magnetic moments and the fact that they are contained in the $\mathbf{a}_m$ - $\mathbf{c}_m$ plane. The same fact is utilized in arriving at the general form of the structure factor, based on the established chemical structure augmented by the operation of time reversal.

(c) With h odd diffraction is by anisotropic components of the orbital octupole moment of a vanadium ion. Such diffraction might be regarded as the magnetic equivalent of Templeton and Templeton scattering from a charge distribution.

(d) Intensities with h even can be used to determine the canting angle, ϕ, of the magnetic easy-axis. Our analysis of data gathered at the pre-edge (5.464 keV) and $(2\bar{2}1)_m$ gives $\phi \sim 70°$ and the value is consistent with the analysis of intensities observed in magnetic neutron diffraction [3]. This outcome at the pre-edge, and related success in explaining other features, confirm that it is due mainly to an E2 resonance event.

(e) As a function of the azimuthal-angle the calculated intensity in the channel with unrotated polarization ($\sigma'\sigma$) is two-fold periodic. This prediction and additional detail in calculated ($\sigma'\sigma$) azimuthal-angle scans is found in intensities collected at Bragg reflections $(2\bar{2}1)_m$, $(111)_m$ and $(30\bar{2})_m$.

(f) In general, the dependence on azimuthal-angle of intensities in the rotated channel ($\pi'\sigma$) show no systematic features. With h odd the ($\pi'\sigma$) azimuthal-angle

scans have a quite complicated pattern which essentially reflects the low symmetry (monoclinic) of the crystal below the Néel temperature.

Acknowledgements

Dr. L. Paolasini has answered several enquiries about the execution of the experiments he and his colleagues have made on V_2O_3, and provided unpublished data to enhance our study. We are grateful to Professor E. Balcar, Dr. K. D. Finkelstein, Dr. S. Langridge, Dr. M. W. Long and Dr. U. Staub for continued interest in our work on the interpretation of resonant x-ray Bragg diffraction. One of us (S.W.L.) has benefited from a discussion with Dr. R. M. Moon.

References

1. D. B. McWhan, T. M. Rice, and J. P. Remeika, Phys. Rev. Lett. **23**, 1334 (1969).
2. P. D. Dernier and M. Marezio, Phys. Rev. **B2**, 3771 (1970).
3. R. M. Moon, Phys. Rev. Lett. **25**, 527 (1970).
4. D. B. McWhan et al., Phys. Rev. **B7**, 1920 (1973).
5. N. F. Mott, Metal-Insulator Transitions (Taylor and Francis, London, 1990).
6. T. M. Rice, Spectroscopy of Mott Insulators and Correlated Metals, edited by A. Fujimori and Y. Tokura (Springer, Berlin, 1995).
7. F. Mila et al., Phys. Rev. Lett. **85**, 1714 (2000).
8. L. Paolasini et al., Phys. Rev. Lett. **82**, 4719 (1999).
9. L. Paolasini et al., submitted to J. Elect. Spect. & Related Phenomena (2000).
10. L. Paolasini, private communication.
11. S. W. Lovesey and K. S. Knight, J. Phys.: Condens. Matter **12**, L367 (2000).
12. D. H. Templeton and L. K. Templeton, Phys. Rev. **B49**, 14850 (1994).
13. D. H. Templeton, Acta Cryst. **A54**, 158 (1998).
14. K. D. Finkelstein, Q. Shen and S. Shastri, Phys. Rev. Lett. **69**, 1612 (1992).
15. Y. Tanaka et al., J. Phys.: Condens. Matter **11**, L505 (1999).
16. S. W. Lovesey, J. Phys.: Condens. Matter **10**, 2505 (1998).
17. S. W. Lovesey, K. S. Knight and E. Balcar, to appear in Phys. Rev. **B** (2001).
18. D. A. Varshalovich, A. N. Moskalev and V. K. Khersonskii, Quantum Theory of Angular Momentum (World Scientific, Singapore, 1988).
19. E. Balcar, S. W. Lovesey and F. A. Wedgwood, J. Phys. C: Solid State Phys. **6**, 3746 (1973).
20. D. S. Sivia, Data Analysis – A Bayesian Tutorial (Oxford University Press, Oxford, 1996).
21. J. A. Nelder and R. Mead, Computer J. **7**, 308 (1965).

Figure Captions

Fig. 1

Positions of the eight vanadium ions in the monoclinic unit cell together with the configuration of their magnetic moments which lie in the $\mathbf{a}_m - \mathbf{c}_m$ plane of the diagram. The monoclinic Bragg wavevector $(20\bar{2})_m$ is parallel to the trigonal axis $\mathbf{c}_h$, and $\mathbf{b}_m$ is normal to the plane of the diagram and parallel to $\mathbf{a}_h$.

Fig. 2

The orthogonal states of polarization in the primary beam of x-rays with σ-polarization normal to the plane of scattering defined by the primary ($\mathbf{q}$) and diffracted ($\mathbf{q}'$) wavevectors. X-rays are deflected through an angle 2θ and $\boldsymbol{\tau}_m = \mathbf{q} - \mathbf{q}'$. Orthogonal axes ($x$, y, z) are related to the geometry of the experiment; the **x**-axis is parallel to $-\boldsymbol{\tau}_m$ and the **z**-axis is normal to the plane of scattering and parallel to σ-polarization. An azimuthal-angle scan is rotation of the crystal by ψ about $\boldsymbol{\tau}_m$, and the origin $\psi = 0$ is defined by a specified plane normal to the plane of scattering.

Fig. 3

Data gathered at the $(2\bar{2}1)_m$ reflection from V_2O_3, with 2.8% Cr doping, at 100K [9]. The continuous curves are generated from expressions (4.5) and (4.6) with a Bragg angle $\theta = 36.9°$ ($\lambda = 2.27$Å). From data gathered in the unrotated channel ($\sigma'\sigma$) the fit gives $\phi = 66.1° \pm 2.1°$ and $\langle \Lambda_0 \rangle_m / 3\langle L_0 \rangle_m = 0.00 \pm 0.05$; the corresponding values obtained from data in the rotated channel ($\pi'\sigma$) are $\phi = 75.7° \pm 1.8°$ and $\langle \Lambda_0 \rangle_m / 3\langle L_0 \rangle_m = -0.06 \pm 0.01$.

Fig. 4

Data on Cr-doped V_2O_3 held at temperature = 0.55 T_N = 100K, and $\boldsymbol{\tau}_m = (111)_m$ with $\theta = 20.8°$ [8]. From data in the unrotated channel and (4.9) we find $r = 0.33 \pm 0.04$ and $t = -0.35 \pm 0.15$, and from data in the rotated channel and (4.10) we find $r = 0.36 \pm 0.02$ and $t = -1.00 \pm 0.13$.

Table I

Components entering the structure factor of V_2O_3 in the monoclinic structure. The eight vanadium ions are labelled according to the scheme shown in Fig. 1, and $h + k + l$ is an odd integer. The angles appearing in the spatial phase factors are $\nu = 2\pi\,(xh + yk + zl)$ and $\varepsilon = 4\pi yk$, and values for (x, y, z) are mentioned in section 2.

Site Label	Spatial Phase factor	Atomic tensor
(1)	$e^{i\nu}$	$\langle T_Q^{(K)}(1)\rangle$
(2)	$-e^{i\nu}$	$(-1)^K\langle T_Q^{(K)}(1)\rangle$
(3)	$e^{i(\varepsilon-\nu+\pi h)}$	$\langle T_Q^{(K)}(3)\rangle$
(4)	$-e^{i(\varepsilon-\nu+\pi h)}$	$(-1)^K\langle T_Q^{(K)}(3)\rangle$
(5)	$e^{-i\nu}$	$\langle T_Q^{(K)}(5)\rangle$
(6)	$-e^{-i\nu}$	$(-1)^K\langle T_Q^{(K)}(5)\rangle$
(7)	$e^{i(\nu+\pi h\,-\,\varepsilon)}$	$\langle T_Q^{(K)}(7)\rangle$
(8)	$-e^{i(\nu+\pi h\,-\,\varepsilon)}$	$(-1)^K\langle T_Q^{(K)}(7)\rangle$

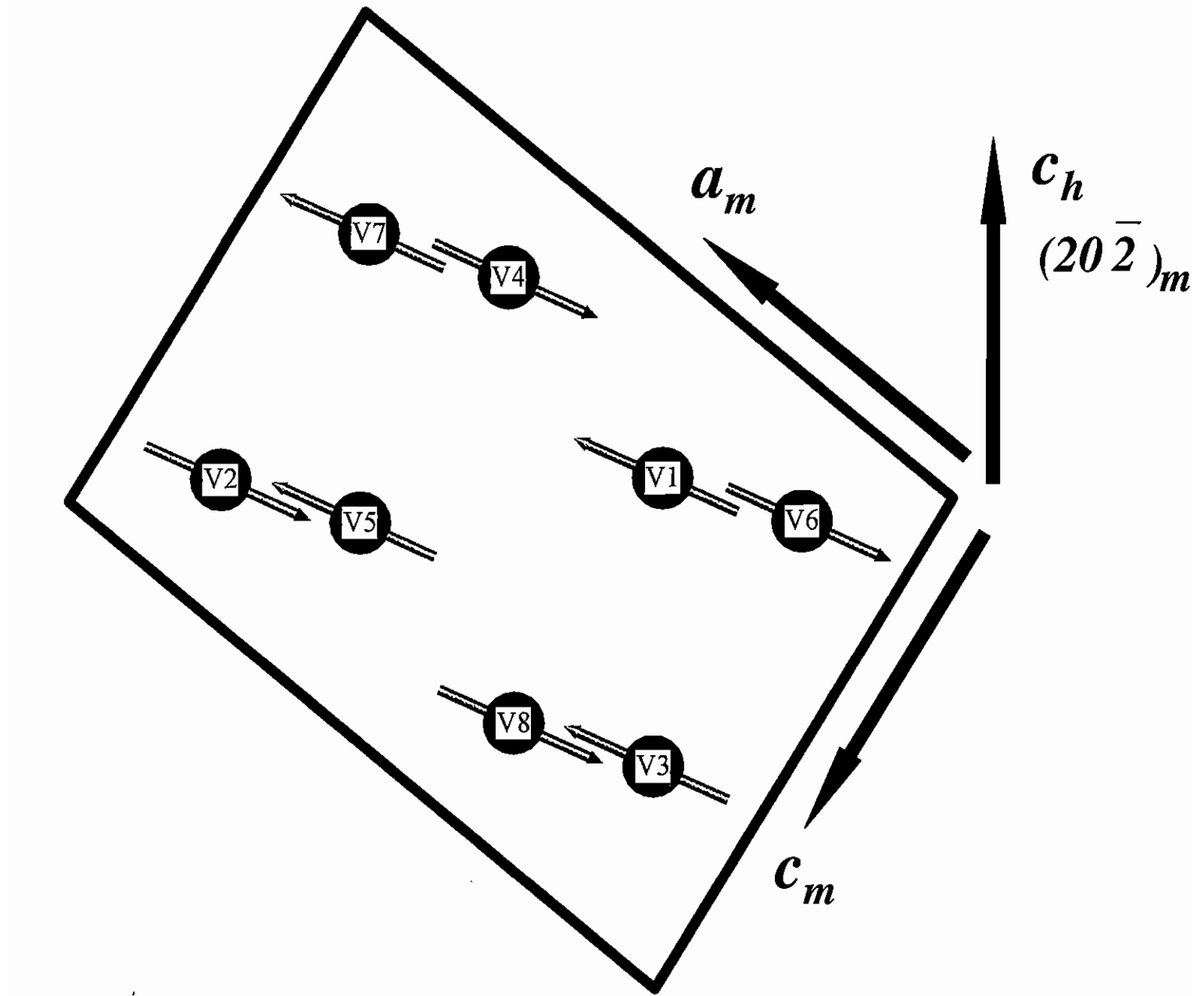

Fig. 1

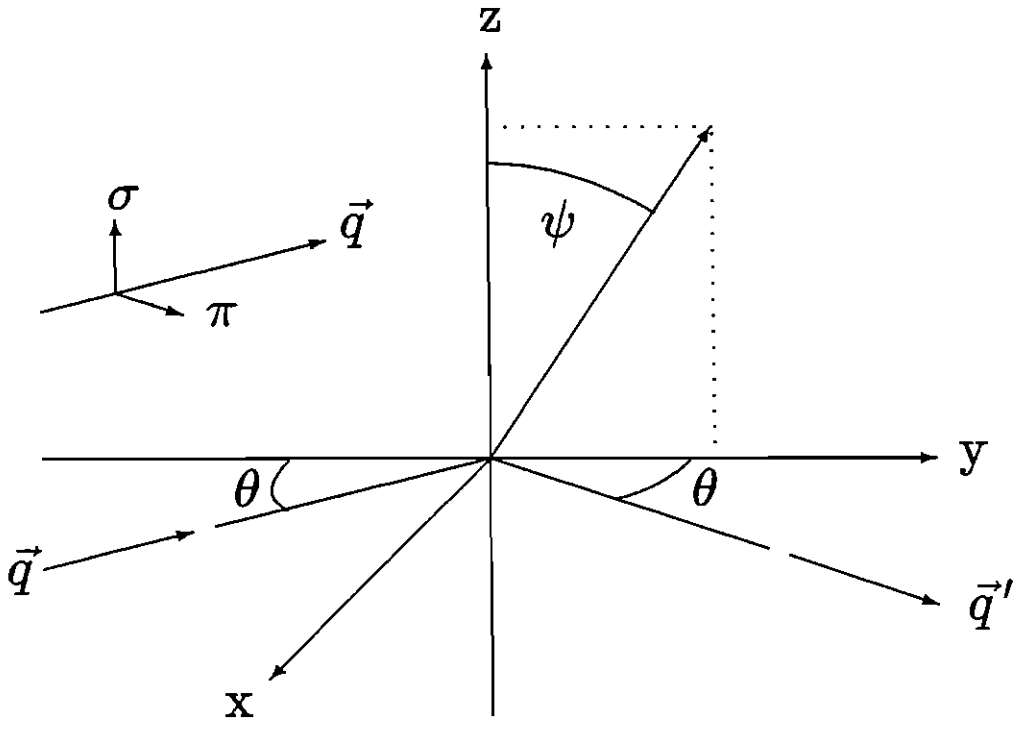
z
σ
$\vec{q}$
π
ψ
y
θ
θ
$\vec{q}$
$\vec{q}'$
x

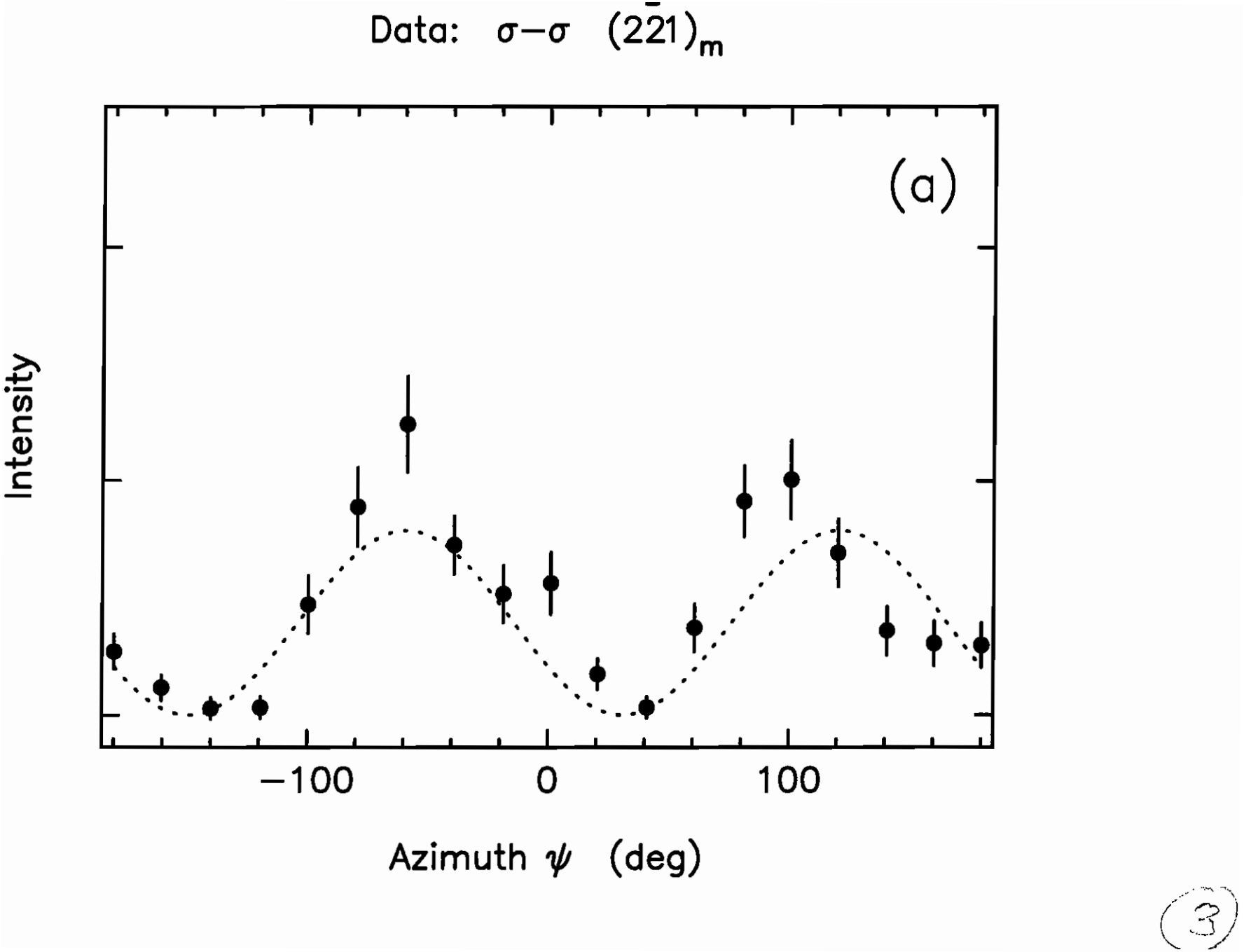
Data: σ−σ (2$\bar{2}$1)$_m$
(a)
Intensity
−100
0
100
Azimuth ψ (deg)

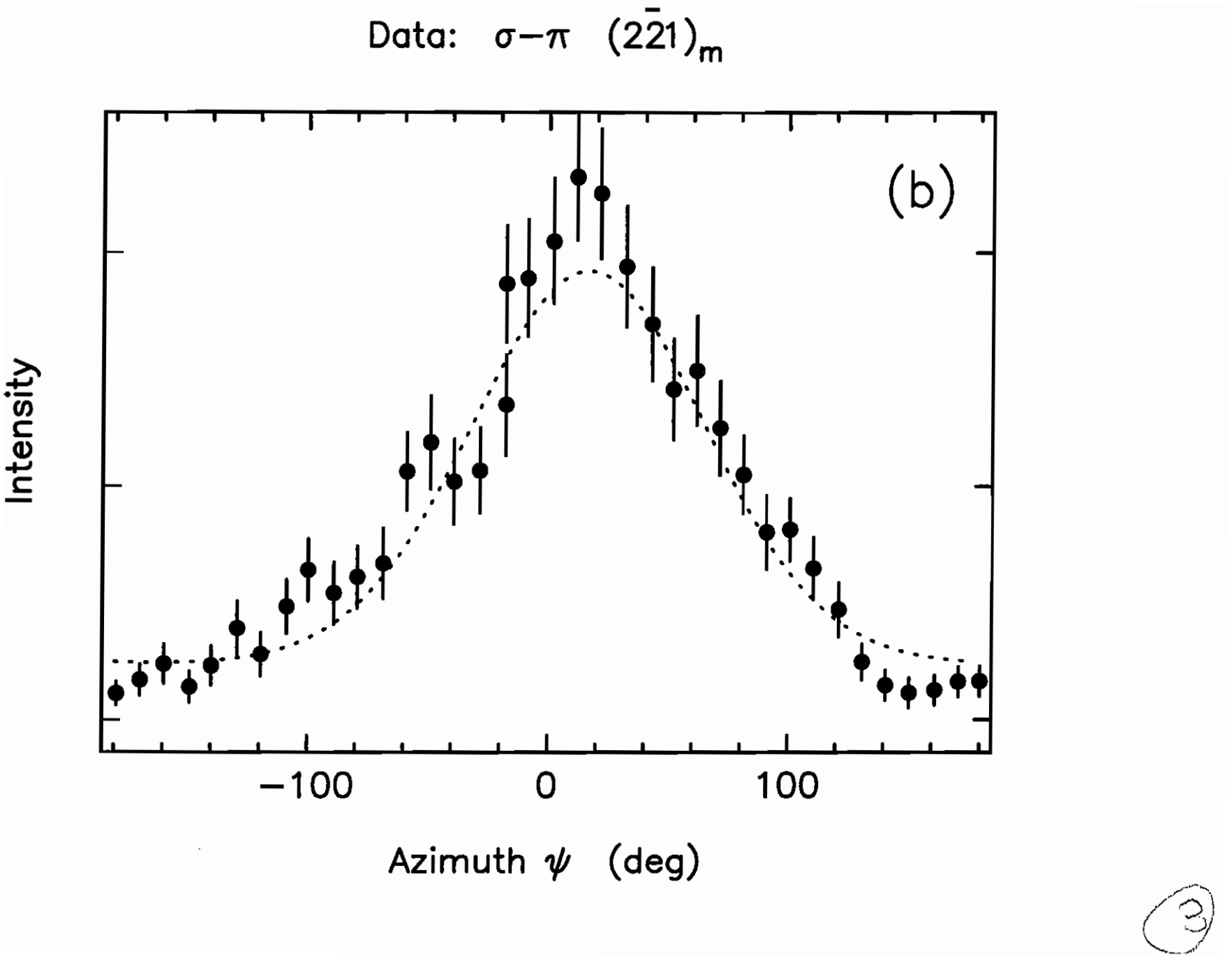
Data: σ−π (2$\bar{2}$1)$_m$
(b)
Intensity
−100
0
100
Azimuth ψ (deg)

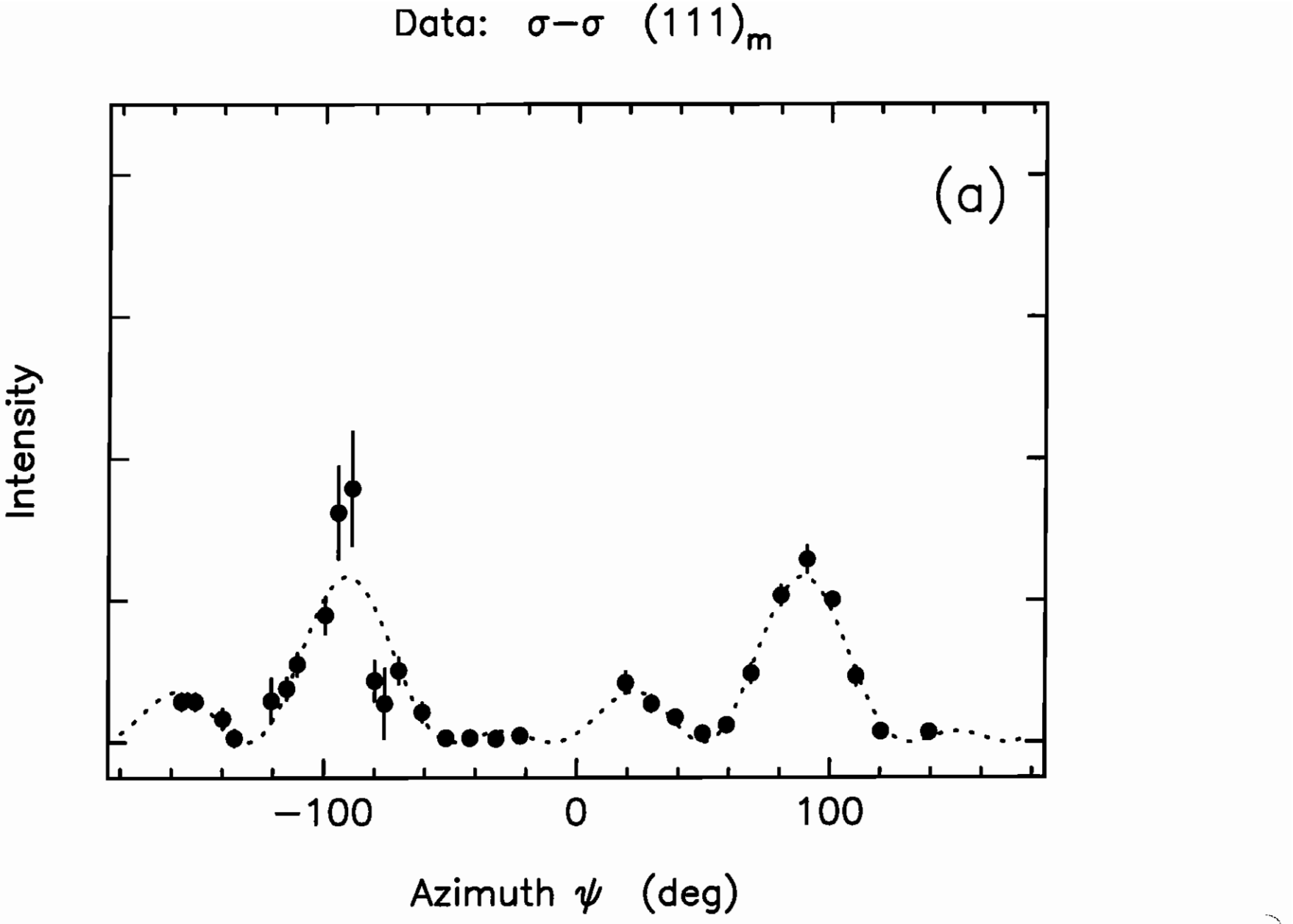
Data: σ−σ (111)m
(a)
Intensity
−100
0
100
Azimuth ψ (deg)

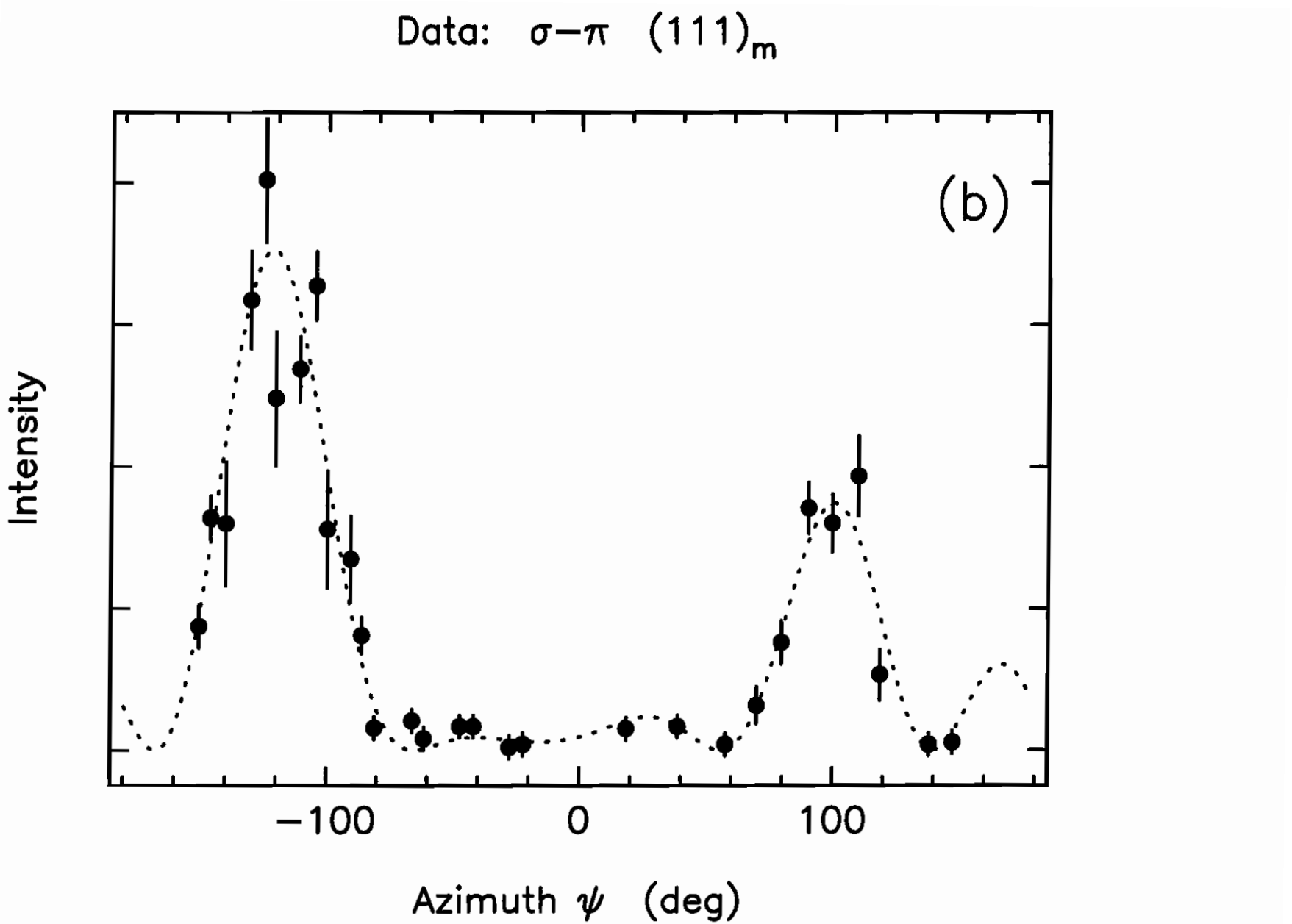
Data: σ−π (111)m
(b)
Intensity
−100
0
100
Azimuth ψ (deg)